

# $p$ orbitals in 3D lattices; fermions, bosons and (exotic) models of magnetism

Fernanda Pinheiro\*

*Department of Physics, Stockholm University, Se-106 91 Stockholm, Sweden and  
NORDITA, KTH Royal Institute of Technology and Stockholm University, Se-106 91 Stockholm, Sweden  
(Dated: October 30, 2014)*

We demonstrate how different types of  $SU(3)$  Heisenberg models can be implemented with the use of the  $p$  orbitals of three dimensional optical lattices. By considering a Mott insulator with unit filling, the dynamics is well described by an effective model derived from the perturbative treatment of the tunneling elements relative to the onsite interaction terms. This yields systems with degrees of freedom that are generators of the  $SU(3)$  group, which extends the Heisenberg models frequently used to analyze quantum magnetism. Due to the different character of interactions in the bosonic and fermionic cases, the choice of atom determines what type of anisotropies will appear in the couplings of the corresponding effective Hamiltonians. Experimental schemes for detection and manipulation of these systems are presented, and properties of the ground states of selected examples are discussed.

PACS numbers: 03.75.Lm, 67.85.Hj, 05.30.Rt

## I. INTRODUCTION

The amazing degree of control and manipulation in experiments with systems of cold atoms has recently awoken a renewal of interest in the physics of interacting spins beyond spin  $1/2$  [1–3]. This follows the success with implementation of (spin- $1/2$ ) models of magnetism in the lab [4–7], and opens a great window for application of quantum simulators. A question of great relevance that therefore arises is: what are the experimentally feasible many-body systems that can be used to mimic the physics of particular models of interacting spins? (And how?)

Along these lines, realizations of  $SU(N)$  Heisenberg models have been proposed with fermionic atoms in optical lattices [1–3]. In these systems, the pseudospin degree of freedom is encoded in the nuclear spin states, whose number  $N$  determines the  $SU(N)$  symmetry of the corresponding model [8]. Furthermore, different setups have been suggested with trapped ions for the implementation of the spin 1  $XY$  Hamiltonian [9], and of  $SU(3)$  chains with long-range interaction [10]. Realizations of  $SU(3)$  Heisenberg models with bosonic Mott insulators with spin-orbit coupling have also been proposed [11].

In this paper, we present an alternative controllable system for realization of different types of  $SU(3)$  Heisenberg models. We show that the effective dynamics of the Mott phase with one atom per site (Mott<sub>1</sub>) in the first excited bands of 3D optical lattices is equivalent to that of a system of nearest neighbours interactions, where the degrees of freedom are the generators of the  $SU(3)$  group. Rather than internal electronic atomic states, the pseudospin is encoded here in the vibrational states which correspond to the (onsite)  $p$  orbitals of the optical potential. In 3D, the first excited bands, or  $p$  band, can be made 3-fold degenerate. This is the case, for example, in

the cubic lattice, where the three orbital states, generally called  $p_x$ ,  $p_y$  and  $p_z$  orbitals, are anisotropic both in magnitude and parity [12, 13]. As a consequence, the dynamics of many-body systems in the  $p$  band can be considerably different than multispecies systems in the ground or  $s$  band. It is characterized by anisotropic tunneling amplitudes, and in addition to density-density interactions, the bosonic case features processes that transfer population between the different orbital states. These additional properties have already been shown to have important effects for the bosonic Mott phase with one particle per site in 2D optical lattices, for its effective dynamics corresponds to that of the fully anisotropic spin- $1/2$  Heisenberg model in an external field [14].

Our focus here is the physics of the Mott<sub>1</sub> phase in the  $p$  band of 3D optical lattices, which is 3-fold degenerate (or quasi-degenerate). We study different systems in terms of their corresponding effective Hamiltonians, obtained from the perturbative treatment of tunneling elements up to second order. We will extend the method used in Ref. [14] to account for the 3-orbital case and we discuss properties of both the fermionic and the bosonic cases. As will be shown, the statistics of the atoms play an important role in determining the anisotropies in the couplings of the effective Hamiltonians. We will also characterize the ground states in of the some specific cases. For antiferromagnetic  $SU(3)$  Heisenberg models, very rich physics is expected from competition between quantum and classical fluctuations [1, 2], which lead to the formation of ground states with 2 and 3-sublattice ordering both in 2D and 3D [1, 2, 15]. In the ferromagnetic case, we look for ground states which feature spiral spin textures, as recently reported in Ref. [11].

The paper is organized as follows: In Sec. II we discuss the Hamiltonians of both the many-body bosonic and fermionic systems in the  $p$ -band. We then derive the effective Hamiltonians for the Mott<sub>1</sub> phase in Sec. III and discuss properties of the ground states in some special cases. Sec. IV is devoted to experimental probing

---

\* fep@fysik.su.se

of these systems, and in Sec. V we discuss the effects of imperfections in experimental realization. Final remarks and further extensions of the techniques considered here are discussed in the Conclusions.

## II. DYNAMICS IN THE $p$ BAND

We start with the general expression of the many-body Hamiltonian in terms of the field operators,

$$H = \int d\vec{r} \left\{ \hat{\Psi}^\dagger(\vec{r}) \left[ -\frac{\hbar^2}{2m} \nabla^2 + V(\vec{r}) \right] \hat{\Psi}(\vec{r}) + \frac{U_0}{2} \hat{\Psi}^\dagger(\vec{r}) \hat{\Psi}^\dagger(\vec{r}) \hat{\Psi}(\vec{r}) \hat{\Psi}(\vec{r}) \right\}, \quad (1)$$

where  $m$  is the mass of the atoms,  $V(\vec{r})$  accounts for the effects of external potentials in the system and  $U_0 = 4\pi\hbar^2 a/m$ , with  $a$  the  $s$ -wave scattering length, measures the strength of (short-range) contact interactions. The field operators  $\hat{\Psi}(\vec{r})$  and  $\hat{\Psi}^\dagger(\vec{r})$  annihilate and create a particle at the position  $\vec{r}$ , and obey commutation relations  $[\hat{\Psi}(\vec{r}), \hat{\Psi}^\dagger(\vec{r}')] = \delta(\vec{r} - \vec{r}')$  and anti-commutation relations and  $\{\hat{\Psi}(\vec{r}), \hat{\Psi}^\dagger(\vec{r}')\} = \delta(\vec{r} - \vec{r}')$  for bosons and fermions, respectively. For the periodic lattice considered here the dynamics is separable in the different directions, i.e.,

$$V(\vec{r}) = V_x \sin^2(k_x x) + V_y \sin^2(k_y y) + V_z \sin^2(k_z z), \quad (2)$$

where  $V_\sigma$  are the amplitudes of the lasers in the direction  $\sigma = \{x, y, z\}$  and  $k_\sigma = 2\pi/\lambda_\sigma$  are the lasers wave vectors, with  $\lambda_\sigma$  the lasers wavelengths. All energies are scaled with the recoil energy,  $E_R = \hbar^2 k_\sigma^2 / 2m$ , for the  $\sigma'$  that defines the smallest  $k_\sigma$ .

Following the usual prescription, we study the physics in the first excited bands of this lattice by expanding the field operators in (1) in terms of the site-localized  $p$  orbitals (or  $p$  bands) [12, 16],

$$\hat{\Psi}(\vec{r}) = \sum_{\mathbf{i}} \sum_{\alpha} \psi_{\alpha, \mathbf{i}}(\vec{r}) \hat{a}_{\alpha, \mathbf{i}}, \quad (3)$$

where  $\alpha = \{x, y, z\}$  and  $\hat{a}_{\alpha, \mathbf{i}}$  annihilates an atom in the  $p_\alpha$ -orbital state at the site  $\mathbf{i} = (i_x, i_y, i_z)$ .

### A. The bosonic case

After expanding the field operators according to (3), and truncating the kinetic terms to its leading contribution, i.e. the tight-binding approximation, the Hamiltonian describing bosonic atoms in the  $p$ -band of a 3D optical lattice is given by

$$\hat{H}_B = \hat{H}_0 + \hat{H}_{nn} + \hat{H}_{nn'} + \hat{H}_{OD}. \quad (4)$$

The first term is the free Hamiltonian

$$\hat{H}_0 = - \sum_{\sigma, \alpha} \sum_{\langle \mathbf{i}, \mathbf{j} \rangle_\sigma} t_{\mathbf{ij}}^\alpha (\hat{a}_{\alpha, \mathbf{i}}^\dagger \hat{a}_{\alpha, \mathbf{j}} + \hat{a}_{\alpha, \mathbf{j}}^\dagger \hat{a}_{\alpha, \mathbf{i}}), \quad (5)$$

that describes the nearest neighbour tunneling of atoms in the  $p_\alpha$ -orbital state,  $\alpha = \{x, y, z\}$ , in the direction  $\sigma = \{x, y, z\}$ . The second and the third terms describe different types of density-density interactions:

$$\hat{H}_{nn} = \sum_{\alpha} \sum_{\mathbf{i}} \frac{U_{\alpha\alpha}}{2} \hat{n}_{\alpha, \mathbf{i}} (\hat{n}_{\alpha, \mathbf{i}} - 1), \quad (6)$$

between atoms in the same orbital state, with  $\hat{n}_{\alpha, \mathbf{i}} = \hat{a}_{\alpha, \mathbf{i}}^\dagger \hat{a}_{\alpha, \mathbf{i}}$ ; and

$$\hat{H}_{nn'} = \sum_{\alpha \neq \beta} \sum_{\mathbf{i}} 2U_{\alpha\beta} \hat{n}_{\alpha, \mathbf{i}} \hat{n}_{\beta, \mathbf{i}}, \quad (7)$$

$\beta = \{x, y, z\}$ , between atoms in different orbital states. The last term

$$\hat{H}_{OD} = \sum_{\alpha \neq \beta} \sum_{\mathbf{i}} \frac{U_{\alpha\beta}}{2} (\hat{a}_{\alpha, \mathbf{i}}^\dagger \hat{a}_{\alpha, \mathbf{i}}^\dagger \hat{a}_{\beta, \mathbf{i}} \hat{a}_{\beta, \mathbf{i}} + \hat{a}_{\beta, \mathbf{i}}^\dagger \hat{a}_{\beta, \mathbf{i}}^\dagger \hat{a}_{\alpha, \mathbf{i}} \hat{a}_{\alpha, \mathbf{i}}) \quad (8)$$

describes interactions that transfer population within different types of orbital states. This is a key ingredient for characterizing collective properties of bosons in the  $p$  band. It reduces the  $U(1) \times U(1) \times U(1)$  global symmetry of the model to  $U(1) \times Z_2 \times Z_2$ , and as a consequence, total population of each of the orbital states is conserved only modulo 2. It has also fundamental implications, for it prevents the Hohenberg-Mermin-Wagner theorem [17, 18] from prohibiting long-range phase coherence in low dimensional systems of bosons in the  $p$  band.

In terms of the orbital states, the expression for the tunneling coefficients in the direction  $\sigma$  is given by

$$t_{\mathbf{ij}}^\alpha = - \int d\vec{r} \psi_{\alpha, \mathbf{i}}^*(\vec{r}) [-\nabla^2 + V(\vec{r})] \psi_{\alpha, \mathbf{j}+1_\sigma}(\vec{r}), \quad (9)$$

and due to the differences in the curvature of the excited bands in the directions perpendicular and parallel to the label of the orbital wave functions,  $t_\perp t_\parallel < 0$ , where  $t_\perp$  and  $t_\parallel$  refer, respectively, to the perpendicular and parallel tunnelings. Notice furthermore that the label of the orbital state is a reference to the direction which introduces the node in the orbital wavefunction. In the same way, the expression of the interaction coefficients is given by

$$U_{\alpha\beta} = U_0 \int d\vec{r} |\psi_{\alpha, \mathbf{j}}(\vec{r})|^2 |\psi_{\beta, \mathbf{j}}(\vec{r})|^2. \quad (10)$$

As final remark we recall that in the bosonic case  $[\hat{a}_{\alpha, \mathbf{i}}, \hat{a}_{\beta, \mathbf{j}}] = \delta_{\alpha\beta} \delta_{\mathbf{i}, \mathbf{j}}$ .

### B. The fermionic case

Anti-commutation relations prevent the occupation of the same orbital state by more than one identical fermion. Therefore, (spinless) fermionic atoms in the  $p$  band behave according to

$$\hat{H}_F = \hat{H}_0 + \hat{H}_{nn'}, \quad (11)$$

with  $\hat{H}_0$  and  $\hat{H}_{nn'}$  defined in Eqs. (5) and (7), respectively. Here, however,  $\{\hat{a}_{\alpha,i}, \hat{a}_{\beta,j}\} = \delta_{\alpha\beta}\delta_{i,j}$ . The expressions for the tunneling elements and the various coupling constants are the same as in the bosonic case, defined in Eqs. (9) and (10).

### III. EFFECTIVE HAMILTONIAN

We now turn to the physics deep in the Mott<sub>1</sub> phase. In this regime  $|t^{\alpha\alpha}| \ll U_{\alpha\beta}$  and the dynamics can be effectively described by a Hamiltonian where the tunneling processes are treated/included perturbatively [19]. This effective Hamiltonian is most easily derived by introducing the  $\hat{P}$  and  $\hat{Q}$  projectors,  $\hat{P} + \hat{Q} = 1$ ,  $\hat{P}^2 = \hat{P}$  and  $\hat{Q}^2 = \hat{Q}$ , that project, respectively, into Hilbert space of states with singly occupied sites,  $\mathcal{H}_P$ , and the states that have at least one site with double occupation,  $\mathcal{H}_Q$ . The eigenvalue problem  $\hat{H}\Psi = E\Psi$  can then be written as

$$\hat{H}(\hat{P} + \hat{Q})\Psi \rightarrow (\hat{H}_K + \hat{H}_U)(\hat{P} + \hat{Q})\Psi = E\Psi, \quad (12)$$

where  $\hat{H}_K = \hat{H}_0$  is the kinetic part of Eq. (4), and  $\hat{H}_U$  is the interaction Hamiltonian. Now acting from the left with the projectors on Eq. (12),

$$(\hat{Q}\hat{H}_K\hat{P} + \hat{Q}\hat{H}_K\hat{Q} + \hat{Q}\hat{H}_U\hat{P} + \hat{Q}\hat{H}_U\hat{Q})\Psi = E\hat{Q}\Psi, \quad (13)$$

$$(\hat{P}\hat{H}_K\hat{P} + \hat{P}\hat{H}_K\hat{Q} + \hat{P}\hat{H}_U\hat{Q} + \hat{Q}\hat{H}_U\hat{P})\Psi = E\hat{P}\Psi. \quad (14)$$

$\hat{Q}\hat{H}_K\hat{Q}$  and  $\hat{P}\hat{H}_U\hat{P}$  are identically zero for computing overlaps between elements projected in disjoint subspaces of the Hilbert space.  $\hat{P}\hat{H}_U\hat{P}$  is also zero because it computes interactions in singly occupied sites. We then obtain

$$\hat{Q}\Psi = -\frac{1}{\hat{Q}\hat{H}_Q - E}\hat{Q}\hat{H}_K\hat{P}\Psi, \quad (15)$$

which leads to

$$\hat{H}_{Mott_1} = -\hat{P}\hat{H}_K\hat{Q}\frac{1}{\hat{Q}\hat{H}_Q - E}\hat{Q}\hat{H}_K\hat{P}. \quad (16)$$

So far this expression is free from approximations and will serve as the starting point in the derivation of the effective Hamiltonian describing the Mott<sub>1</sub> phase of the systems considered here. This language is particularly

useful for highlighting the role of the tunneling elements, namely of connecting the intermediate and final states of the perturbative process in the  $\mathcal{H}_Q$  and  $\mathcal{H}_P$  subspaces, respectively.

Now the assumption of a Mott phase justify expanding the operator  $1/(\hat{Q}\hat{H}_Q - E)$  to second order in  $t/U$ , and due to the tight-binding regime it is enough to consider the 2-site problem. We then define the basis spanning the subspace of states with unit filling as

$$\mathcal{H}_P = \{|x, x\rangle, |x, y\rangle, |x, z\rangle, |y, y\rangle, |y, z\rangle, |z, x\rangle, |z, y\rangle, |z, z\rangle\}, \quad (17)$$

where  $|\alpha, \beta\rangle = \hat{a}_{\alpha,i}^\dagger \hat{a}_{\beta,j}^\dagger |0\rangle$ , corresponds to the state with a  $p_\alpha$  orbital in the site  $i$  and a  $p_\beta$  orbital in the neighbouring site  $j$ ,  $\alpha, \beta = \{x, y, z\}$ .

In the same way, the relevant states in the basis of the subspace of doubly occupied sites follow

$$\mathcal{H}_Q = \{|0, 2x\rangle, |0, 2y\rangle, |0, 2z\rangle, |0, xy\rangle, |0, xz\rangle, |0, yz\rangle\}, \quad (18)$$

with  $|0, 2\alpha\rangle = 2^{-1/2} \hat{a}_{\alpha,j}^\dagger \hat{a}_{\alpha,j}^\dagger |0\rangle$  and  $|0, \alpha\beta\rangle = \hat{a}_{\alpha,j}^\dagger \hat{a}_{\beta,j}^\dagger |0\rangle$ . Notice that due to the restrictions imposed by the exclusion principle, the relevant part of the basis in the  $\mathcal{H}_Q$  subspace of the fermionic problem is only composed of the  $|0, \alpha\beta\rangle = \hat{a}_{\alpha,j}^\dagger \hat{a}_{\beta,j}^\dagger |0\rangle$  states with  $\alpha \neq \beta$ . This leads to important differences when deriving the effective Hamiltonians of the bosonic and fermionic cases and will be discussed in greater detail in the following sections.

#### A. The effective Hamiltonian for bosons

Due to the nonvanishing contributions of the orbital changing processes in the states of the type  $|0, 2\alpha\rangle = 2^{-1/2} \hat{a}_{\alpha,j}^\dagger \hat{a}_{\alpha,j}^\dagger |0\rangle$  in the bosonic case, the projection of the Hamiltonian in the  $\mathcal{H}_Q$  subspace is non-diagonal in the basis of intermediate states of the perturbation theory. As a consequence, we obtain  $(\hat{H}_Q - E)^{-1}$ , with  $\hat{H}_Q = \hat{Q}\hat{H}\hat{Q}$  by first projecting the Hamiltonian in the  $\mathcal{H}_Q$  subspace, and then taking the contributions for the corresponding processes from the inverse of the resulting matrix. In addition, since  $E \sim t^2/U$  we take  $(\hat{H}_Q - E)^{-1} \approx \hat{H}_Q^{-1}$ .

With the basis of  $\mathcal{H}_Q$  ordered according to (18), the projected Hamiltonian  $\hat{H}_Q$  can be written in block diagonal form of 3x3 matrices as

$$H_Q = \begin{pmatrix} H_{Q_1} & 0 \\ 0 & H_{Q_2} \end{pmatrix}, \quad (19)$$

where the first block captures the action of  $\hat{H}_U = \hat{H}_{nn} + \hat{H}_{nn'} + \hat{H}_{OD}$  (recall the definitions in Eqs. (6), (7) and (8)) in the states of the type  $|0, 2\alpha\rangle$ , while the second block accounts for the effects of  $\hat{H}_U$  in the  $|0, \alpha\beta\rangle$  states. The

explicit expressions follow,

$$H_{Q_1} = \begin{pmatrix} U_{xx} & U_{xy} & U_{xz} \\ U_{xy} & U_{yy} & U_{yz} \\ U_{xz} & U_{yz} & U_{zz} \end{pmatrix} \quad (20)$$

and

$$H_{Q_2} = \begin{pmatrix} 2U_{xy} & 0 & 0 \\ 0 & 2U_{xz} & 0 \\ 0 & 0 & 2U_{yz} \end{pmatrix}, \quad (21)$$

from which  $\hat{K} = \hat{H}_Q^{-1}$  is easily computed. In the first block, the elements of  $\hat{K}^{(1)} = \hat{H}_{Q_1}^{-1}$  can be written as

$$\begin{aligned} K_{\alpha\alpha}^{(1)} &= \frac{1}{2\Lambda} \sum_{\beta\gamma} (\epsilon^{\alpha\beta\gamma})^2 (U_{\beta\beta}U_{\gamma\gamma} - U_{\beta\gamma}^2), \\ K_{\alpha\beta}^{(1)} &= \frac{1}{\Lambda} \sum_{\gamma} (\epsilon^{\alpha\beta\gamma})^2 (U_{\alpha\beta}U_{\beta\gamma} - U_{\alpha\gamma}U_{\gamma\beta}) \end{aligned} \quad (22)$$

where  $\epsilon^{\alpha\beta\gamma}$  is the Levi-Civita symbol and  $\{\alpha, \beta, \gamma\} = (1, 2, 3)$  whenever  $\{\alpha, \beta, \gamma\} = (x, y, z)$ , and

$$\begin{aligned} \Lambda &= (U_{xx}U_{yy}U_{zz} - U_{xz}^2U_{yy} - U_{yz}^2U_{xx} - U_{xy}^2U_{zz} \\ &\quad + 2U_{xy}U_{xz}U_{yz})^{-1}. \end{aligned} \quad (23)$$

For simplicity, the elements of  $K^{(2)} = \hat{H}_{Q_2}^{-1}$ , in the second block, are denoted by

$$K_{\alpha\beta}^{(2)} = \frac{1}{2U_{\alpha\beta}}, \quad (24)$$

and in the same way,  $\alpha, \beta = (1, 2, 3)$ , whenever  $\alpha, \beta = (x, y, z)$ .

We determine the final form of the effective Hamiltonian by computing the relevant matrix elements of Eq. (16). To this end, we consider in detail all the different cases:

The states of the type  $|\alpha_i, \alpha_j\rangle$ , and the processes

$$\begin{aligned} \hat{a}_{\alpha,i}^\dagger \hat{a}_{\alpha,j} \hat{K} \hat{a}_{\alpha,i}^\dagger \hat{a}_{\alpha,i} |\alpha_i, \alpha_j\rangle &= \hat{a}_{\alpha,i}^\dagger \hat{a}_{\alpha,j} \hat{K} \sqrt{2} |0, 2\alpha_j\rangle \\ &= \sqrt{2} \hat{a}_{\alpha,i}^\dagger \hat{a}_{\alpha,j} \left( K_{\alpha\alpha}^{(1)} |0, 2\alpha_j\rangle + K_{\alpha\beta}^{(1)} |0, 2\beta_j\rangle \right) \\ &= 2K_{\alpha\alpha}^{(1)} |\alpha_i, \alpha_j\rangle, \end{aligned}$$

contribute to the effective Hamiltonian with terms of the type

$$- \sum_{\langle i,j \rangle} \sum_{\alpha, \beta, \gamma} \frac{|t_{ij}^\alpha|^2}{\Lambda} \left[ (\epsilon^{\alpha\beta\gamma})^2 (U_{\beta\beta}U_{\gamma\gamma} - U_{\beta\gamma}^2) \right] \hat{n}_{\alpha,i} \hat{n}_{\alpha,j}.$$

For the same states, and the processes

$$\begin{aligned} \hat{a}_{\beta,i}^\dagger \hat{a}_{\beta,j} \hat{K} \hat{a}_{\alpha,i}^\dagger \hat{a}_{\alpha,i} |\alpha_i, \alpha_j\rangle &= \hat{a}_{\beta,i}^\dagger \hat{a}_{\beta,j} \hat{K} \sqrt{2} |0, 2\alpha_j\rangle \\ &= 2K_{\alpha\beta}^{(1)} |\beta_i, \beta_j\rangle, \end{aligned}$$

the effective Hamiltonian picks the term

$$- \sum_{\langle i,j \rangle} \sum_{\alpha, \beta, \gamma} 2 \frac{t_{ij}^\alpha t_{ji}^\beta}{\Lambda} \left[ (\epsilon^{\alpha\beta\gamma})^2 (U_{\alpha\beta}U_{\beta\gamma} - U_{\alpha\gamma}U_{\gamma\beta}) \right] \times \hat{a}_{\beta,i}^\dagger \hat{a}_{\alpha,i} \hat{a}_{\beta,j}^\dagger \hat{a}_{\alpha,j}. \quad (25)$$

Next we consider the  $|\alpha_i, \beta_j\rangle$  states, with  $\alpha \neq \beta$ . The processes of the type

$$\begin{aligned} \hat{a}_{\alpha,i}^\dagger \hat{a}_{\alpha,j} \hat{K} \hat{a}_{\alpha,i} \hat{a}_{\alpha,i} |\alpha_i, \beta_j\rangle &= \hat{a}_{\alpha,i}^\dagger \hat{a}_{\alpha,j} \hat{K} |0, \alpha_j \beta_j\rangle \\ &= \hat{a}_{\alpha,i}^\dagger \hat{a}_{\alpha,j} K_{\alpha\beta}^{(2)} |0, \alpha_j \beta_j\rangle = K_{\alpha\beta}^{(2)} |\alpha_i, \beta_j\rangle, \end{aligned} \quad (26)$$

contribute to the effective Hamiltonian with

$$- \sum_{\langle i,j \rangle} \sum_{\alpha, \beta \neq \alpha} |t_{ij}^\alpha|^2 \frac{1}{U_{\alpha\beta}} \hat{n}_{\alpha,i} \hat{n}_{\beta,j}.$$

Finally, for the same states and the processes of the type

$$\begin{aligned} \hat{a}_{\beta,i}^\dagger \hat{a}_{\beta,j} \hat{K} \hat{a}_{\alpha,i} \hat{a}_{\alpha,i} |\alpha_i, \beta_j\rangle &= \hat{a}_{\beta,i}^\dagger \hat{a}_{\alpha,j} \hat{K} |0, \alpha_j \beta_j\rangle \\ &= \hat{a}_{\alpha,i}^\dagger \hat{a}_{\alpha,j} K_{\alpha\beta}^{(2)} |0, \alpha_j \beta_j\rangle = K_{\alpha\beta}^{(2)} |\beta_i, \alpha_j\rangle, \end{aligned} \quad (27)$$

the effective Hamiltonian picks the following contribution

$$- \sum_{\langle i,j \rangle} \sum_{\alpha, \beta \neq \alpha} t_{ij}^\alpha t_{ji}^\beta \frac{1}{U_{\alpha\beta}} \hat{a}_{\beta,i}^\dagger \hat{a}_{\alpha,i} \hat{a}_{\alpha,j}^\dagger \hat{a}_{\beta,j}.$$

Summing the different contributions, the effective Hamiltonian describing the Mott<sub>1</sub> phase of bosons in the  $p$  band of the three orbital system is given by

$$\begin{aligned} H_{M_1}^b &= - \sum_{\langle i,j \rangle} \sum_{\alpha, \beta, \gamma} \left[ \frac{|t_{ij}^\alpha|^2}{\Lambda} (\epsilon^{\alpha\beta\gamma})^2 (U_{\beta\beta}U_{\gamma\gamma} - U_{\beta\gamma}^2) \hat{n}_{\alpha,i} \hat{n}_{\alpha,j} \right. \\ &\quad + 2 \frac{t_{ij}^\alpha t_{ji}^\beta}{\Lambda} (\epsilon^{\alpha\beta\gamma})^2 (U_{\alpha\beta}U_{\beta\gamma} - U_{\alpha\gamma}U_{\gamma\beta}) \hat{a}_{\beta,i}^\dagger \hat{a}_{\alpha,i} \hat{a}_{\beta,j}^\dagger \hat{a}_{\alpha,j} \\ &\quad \left. + \frac{|t_{ij}^\alpha|^2}{U_{\alpha\beta}} \hat{n}_{\alpha,i} \hat{n}_{\alpha,j} + \frac{t_{ij}^\alpha t_{ji}^\beta}{U_{\alpha\beta}} \hat{a}_{\beta,i}^\dagger \hat{a}_{\alpha,i} \hat{a}_{\alpha,j}^\dagger \hat{a}_{\beta,j} \right]. \end{aligned} \quad (28)$$

This is a main result of this paper. We now use the orbital states to define the representation of the  $SU(3)$  group in terms of the Gell-Mann matrices  $\lambda_i$ ,  $i = 1, \dots, 8$  [20]. Although individually the orbital states have the structure of angular momentum, the generators of the  $SU(2)$  group fail to give a description of the effective dynamics of the many-body system with three orbitals in the  $p$  band. The reason is that dynamical processes in the  $p$  band treat any combination of different orbital states at the same footing. As a consequence, the ladder operators act as in the Lie algebra of the  $SU(3)$  group (see Fig. 1).

Using the condition that  $\hat{n}_{x,i} + \hat{n}_{y,i} + \hat{n}_{z,i} = 1$  in the Mott<sub>1</sub> phase, the diagonal elements  $\lambda_3 = \text{diag}(1, -1, 0)$

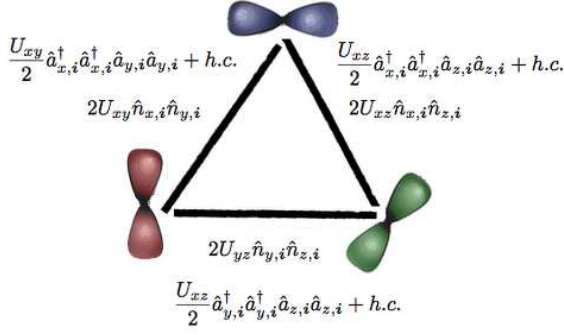


FIG. 1. (Color online) Dynamical processes relating the different orbital states in the many-body bosonic system (as discussed in Eq. (11), the fermionic case contains only the density-density interactions part). Since the different orbitals are treated at the same footing, the effective Hamiltonian describing the many-body system in the  $p$  band with three orbitals requires description in terms of the generators of the  $SU(3)$  group. In fact, in the language of  $p$  orbitals, rather than the triangular scheme displayed above, the ladder operators of a three-state system with  $SU(2)$  symmetry act as  $p_\alpha \rightleftharpoons p_\beta \rightleftharpoons p_\gamma$ .

and  $\lambda_8 = 1/\sqrt{3} \text{diag}(1, 1, -2)$  can be written as

$$\begin{aligned} \hat{n}_{x,i} &= \frac{1}{3} + \frac{1}{2} \lambda_{3,i} + \frac{\sqrt{3}}{6} \lambda_{8,i} \\ \hat{n}_{y,i} &= \frac{1}{3} - \frac{1}{2} \lambda_{3,i} + \frac{\sqrt{3}}{6} \lambda_{8,i} \\ \hat{n}_{z,i} &= \frac{1}{3} - \frac{\sqrt{3}}{6} \lambda_{8,i}. \end{aligned} \quad (29)$$

The  $SU(3)$  ladder operators are defined in terms of the non-diagonal Gell-Mann matrices (see Appendix A for explicit expressions). In terms of the orbital states,

$$\begin{aligned} \frac{\hat{T}_i^\pm}{2} &= \hat{a}_{x,i}^\dagger \hat{a}_{y,i} = \lambda_{z,i}^1 \pm i \lambda_{z,i}^2 \\ \frac{\hat{V}_i^\pm}{2} &= \hat{a}_{x,i}^\dagger \hat{a}_{z,i} = \lambda_{y,i}^1 \pm i \lambda_{y,i}^2 \\ \frac{\hat{U}_i^\pm}{2} &= \hat{a}_{z,i}^\dagger \hat{a}_{y,i} = \lambda_{x,i}^1 \pm i \lambda_{x,i}^2, \end{aligned} \quad (30)$$

where we simplified notation by relabelling the Gell-Mann matrices with the index of the symmetry axis of rotation of the corresponding  $SU(2)$  subalgebra. In the usual setting  $\lambda_z^1 = \lambda^1$ ,  $\lambda_z^2 = \lambda_2$ ,  $\lambda_y^1 = \lambda^4$ ,  $\lambda_y^2 = \lambda_5$ ,  $\lambda_x^1 = \lambda^6$  and  $\lambda_x^2 = \lambda_7$ .

This allows the Hamiltonian (28) to be written in a more compact form,

$$\begin{aligned} \hat{H}_{M_1}^b &= - \sum_{\sigma} \sum_{\langle i,j \rangle_{\sigma}} \left[ J_{3,\sigma}^b \lambda_{3,i} \lambda_{3,j} + J_{8,\sigma}^b \lambda_{8,i} \lambda_{8,j} \right. \\ &\quad \left. + J_{38,\sigma}^b (\lambda_{3,i} \lambda_{8,j} + \lambda_{8,i} \lambda_{3,j}) \right. \\ &\quad \left. + \sum_{\gamma} J_{\gamma,\sigma}^1 \lambda_{\gamma,i}^1 \lambda_{\gamma,j}^1 + J_{\gamma,\sigma}^2 \lambda_{\gamma,i}^2 \lambda_{\gamma,j}^2 \right] \\ &\quad - \sum_i \left( h_3^b \lambda_{3,i} + h_8^b \lambda_{8,i} \right). \end{aligned} \quad (31)$$

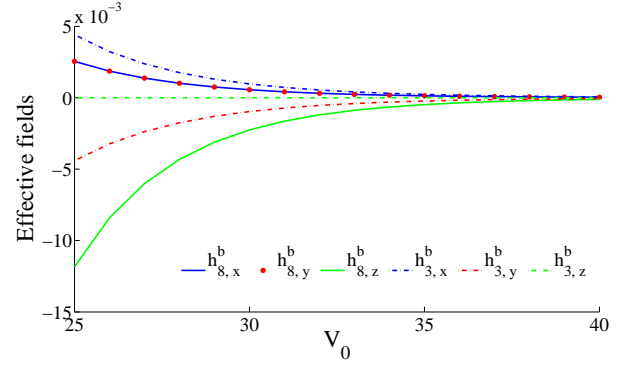


FIG. 2. (Color online) Effective fields for the bosonic system. The indices labeling different directions are used here to illustrate the contribution of external field terms in asymmetric lattices (see discussion in Sec. III C), i.e., where effective 1D and 2D systems are obtained by suppressing the tunneling in 2 or 1 directions. In particular, due to the symmetries of the dynamics in cubic lattices, the term associated to  $h_3^b = h_{3,x}^b + h_{3,y}^b$  vanishes.

Explicit expressions of the coupling constants are not very informative at first sight and can be found in Appendix B. The physics of the system is summarized here, however, from the study of the couplings as a function of the lattice depth, as illustrated in Figs. 2 - 6. They are computed from diagonalization of the Mathieu equation for the potential (2) with  $V_\sigma = V_0$ ,  $\sigma = x, y, z$ , which yields the lattice Wannier functions used in the construction of the  $p$  orbitals. In the same way as  $V_0$ , all the couplings and external fields are scaled with  $E_R$ .

First, due to the tunneling anisotropy, the values of the coupling constants will depend on the direction of dynamics. This system contains two external fields  $h_3^b$  and  $h_8^b$ , associated to  $\lambda_3$  and  $\lambda_8$ , that are shown in Fig. 2. These are, respectively, the isospin and hypercharge operators in the study of strong interactions in QCD, whose eigenvalues are used to label the states of the  $SU(3)$  multiplet [20]. In the context of  $p$ -band physics, the external fields are related to population imbalance in the different orbital states at each site. In order to connect this notation with the one used in Fig. 2, we notice that  $h_8^b = \sum_{\sigma} h_{8,\sigma}^b$  and  $h_3^b = \sum_{\sigma} h_{3,\sigma}^b$ . This choice will become more transparent in the discussion of realizations of the effective models in 1D and 2D lattices in Sec. III C. For the moment, however, we remark that as a consequence of the symmetries of the dynamics in the  $p$  band of isotropic cubic lattices, contributions of the  $h_3^b$  external field vanish after summation over  $\sigma$ .

The leading interaction terms in this Hamiltonian stem from contributions of density-density interactions in the bosonic picture, both between atoms in the same and in different orbital states. Here again, due to the symmetries of the dynamics in the  $p$  band  $J_{38,x} = -J_{38,y}$  (see Fig. 3), and therefore the term with coefficient  $J_{38,\sigma}^b$  vanishes after summation over  $\sigma$  in the case of a cubic lattice.



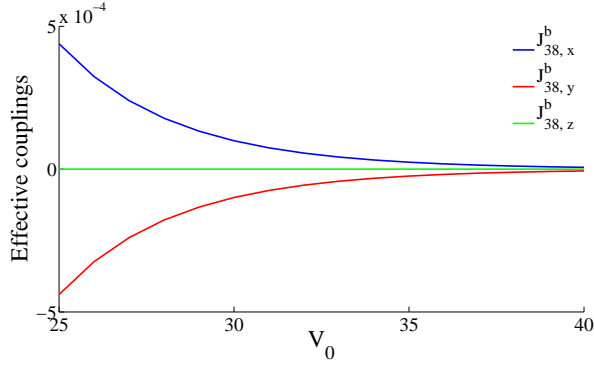


FIG. 3. (Color online) Effective couplings for the nearest neighbour interactions  $(\lambda_{8,i}\lambda_{3,i} + \lambda_{3,i}\lambda_{8,i})$ . In the same way as for the external fields shown in Fig. 2, the relative sign for the couplings of dynamics in the  $x$  and  $y$  directions follow directly from the symmetries in the  $p$  band of isotropic cubic lattices (see details in the text). In addition, these processes vanish in the case of isotropic cubic lattices.

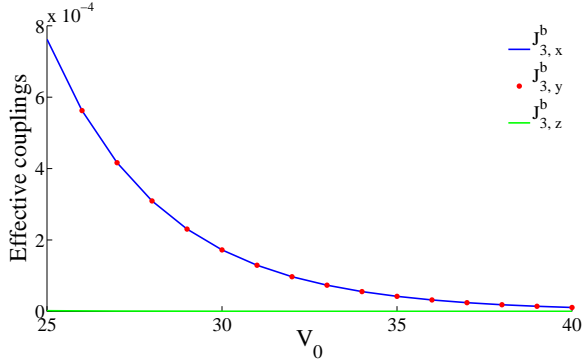


FIG. 4. (Color online) Effective couplings of the bosonic many-body system for  $\lambda_{3,i}\lambda_{3,j}$  interactions in the different directions.

Finally, in the same way as for the effective dynamics of the two-orbital bosonic system in the  $p$  band in Ref. [14], the nearest-neighbour interactions obtained from the ladder operators yield  $XYZ$ -like anisotropies in the couplings of  $\lambda_\gamma^1$  and  $\lambda_\gamma^2$ . As shown in Fig. 6, the directions parallel and perpendicular to  $\gamma$  will have different couplings. However, the symmetries of dynamics in the  $p$  band of cubic lattices imply that  $J_{\gamma,\parallel}^1$  and  $J_{\gamma,\perp}^2$  are the same for all values of  $\gamma = x, y, z$  (recall that  $\gamma$  is the label of the different  $SU(2)$  subalgebras).

### B. The effective Hamiltonian for spinless fermions

The derivation of the effective Hamiltonian describing the Mott<sub>1</sub> phase of fermions in the  $p$  band of 3D lattices is simplified due to the absence of interactions involving two atoms in the same orbital state. Here,  $\hat{H}_Q$  is diagonal in the basis of intermediate states of the perturbative calculation, and the only processes to take into account

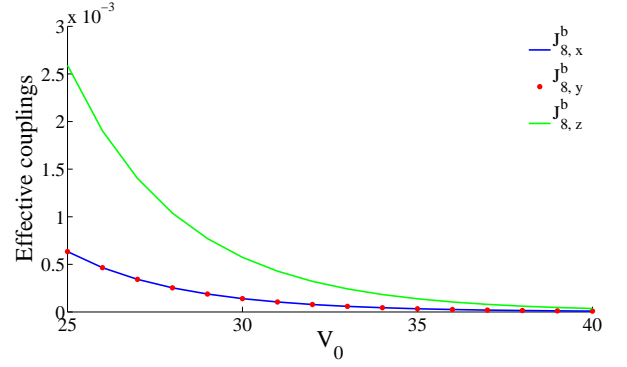


FIG. 5. (Color online) Effective couplings of the bosonic many-body system for  $\lambda_{8,i}\lambda_{8,j}$  interactions in the different directions.

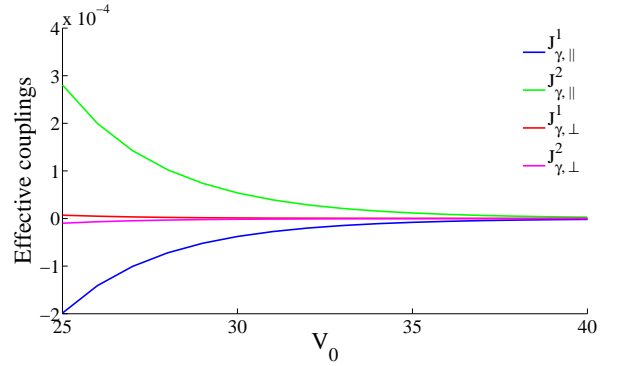


FIG. 6. (Color online) Effective couplings for nearest neighbour interactions obtained from the ladder operators. Notice, in particular, that the couplings associated to the  $\lambda_{\gamma,i}^1\lambda_{\gamma,j}^1$  interactions are not the same as the couplings of  $\lambda_{\gamma,i}^2\lambda_{\gamma,j}^2$ . This is a  $XYZ$ -like anisotropy, which is typical for the bosonic system in the  $p$  band [14]. In fact, this is a direct consequence from the combination of anisotropic tunneling with orbital-changing interaction terms.

are described in Eqs. (26) and (27). Therefore,

$$\hat{H}_{M_1}^f = - \sum_{\langle i,j \rangle} \sum_{\alpha, \beta \neq \alpha} \left[ 2|t_{ij}^\alpha|^2 \frac{1}{2U_{\alpha\beta}} \hat{n}_{\alpha,i} \hat{n}_{\beta,j} + 2t_{ij}^{\alpha\beta} \frac{1}{2U_{\alpha\beta}} \hat{a}_{\beta,i}^\dagger \hat{a}_{\alpha,i} \hat{a}_{\alpha,j}^\dagger \hat{a}_{\beta,j} \right], \quad (32)$$

which in terms of the Gell-Mann matrices (see Eqs. (29) and (30)) becomes

$$\begin{aligned} \hat{H}_{M_1}^f = & - \sum_{\sigma} \sum_{\langle i,j \rangle_{\sigma}} \left[ J_{3,\sigma}^f \lambda_{3,i} \lambda_{3,j} + J_{8,\sigma}^f \lambda_{8,i} \lambda_{8,j} \right. \\ & + J_{38,\sigma}^f (\lambda_{3,i} \lambda_{8,j} + \lambda_{8,i} \lambda_{3,j}) \\ & + \sum_{\gamma} J_{\gamma,\sigma}^f (\lambda_{\gamma,i}^1 \lambda_{\gamma,j}^1 + \lambda_{\gamma,i}^2 \lambda_{\gamma,j}^2) \left. \right] \\ & - \sum_i \left( h_3^f \lambda_{3,i} + h_8^f \lambda_{8,i} \right). \end{aligned} \quad (33)$$

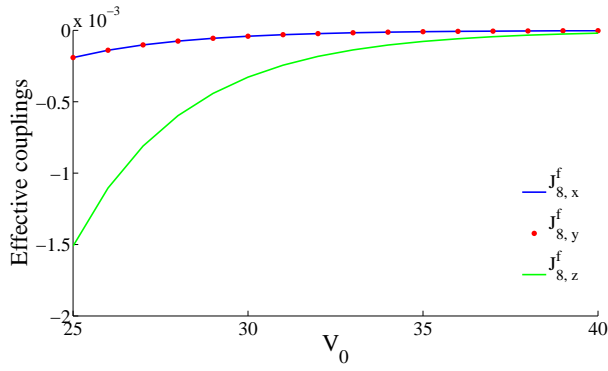


FIG. 7. (Color online)  $J_8^f$  for the fermionic case. Notice here that the  $\lambda_{8,i}\lambda_{8,j}$  term contributes very little for the dynamics in the  $x$  and  $y$  directions, while it is very significant for the dynamics in the  $z$  direction.

Following the analysis of the bosonic case, the expressions of the couplings are given in the Appendix, and the behavior of the couplings as a function of the lattice depths is shown in Figs. 7 - 11. Here too, the leading terms contain contributions deriving from density-density interactions in the many-body system, and are accordingly mediated by the diagonal Gell-Mann matrices. In the fermionic case, however, density-density interactions are only between atoms in different orbital states. In addition, the vanishing of contributions associated to  $h_3^f$  and  $J_{38,\sigma}^f$  in the cubic lattice has the same explanation already discussed for the bosonic case, which is characterized by the same property.

Further comparison between the effective models derived for the many-body bosonic and fermionic systems reveal two main differences. The first one is manifest in the interaction terms derived from contributions of the ladder operators. Namely, the fermionic case lacks the  $XYZ$ -like anisotropy in the couplings of  $\lambda_{\gamma,i}^1\lambda_{\gamma,j}^1$  and  $\lambda_{\gamma,i}^2\lambda_{\gamma,j}^2$ . In fact, the coupling of these terms is much closer in form to the couplings in  $XXZ$   $SU(2)$  Heisenberg models. The second difference is related to the type of ordering preferred for the different systems. While the bosonic case favors ferromagnetic alignment of the degrees of freedom in the leading terms (with couplings  $J_{3,\sigma}^b$  and  $J_{8,\sigma}^b$ ), the fermionic case favors antiferromagnetic alignment (see Figs. 4, 8, 5 and 7).

### C. Different lattices geometries and exotic ground states

Owing to the complexity of these systems, ground-state properties of  $SU(3)$  Heisenberg models have been characterized mainly in systems with isotropic couplings in  $1D$  and  $2D$  [15]. Further studies of both the triangular and the square lattices in  $2D$ , and the cubic lattice in  $3D$  have been carried out numerically only rather recently [1, 2], and complement the previous analysis based

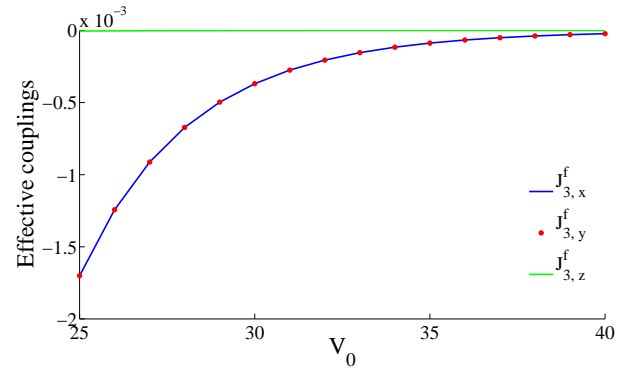


FIG. 8. (Color online) Coefficients of  $\lambda_{3,i}\lambda_{3,j}$  for interactions in the fermionic case in the different directions and as a function of the lattice depth.

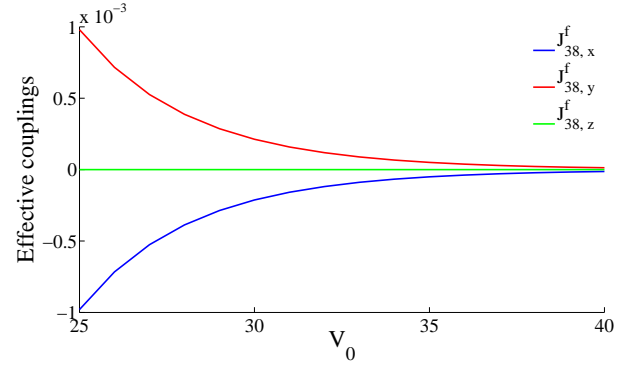


FIG. 9. (Color online) Coefficients of  $(\lambda_{3,i}\lambda_{8,j} + \lambda_{8,i}\lambda_{3,j})$  for the fermionic case. In the same way as discussed in the bosonic case, these terms yield no contribution to the energy in isotropic cubic lattices.

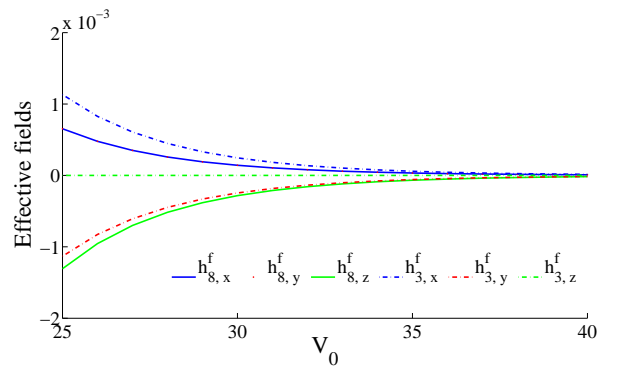


FIG. 10. (Color online) Effective fields of the effective model with fermionic atoms in isotropic cubic lattices. The situation is again similar to what is discussed in the bosonic case in Fig. 2. This should be the case, since the external fields account for single particle contributions and therefore are independent from the statistic of the atoms. In the  $p$ -band system, in particular, the external fields encode the degree of imbalance in the occupation of the different orbital states.

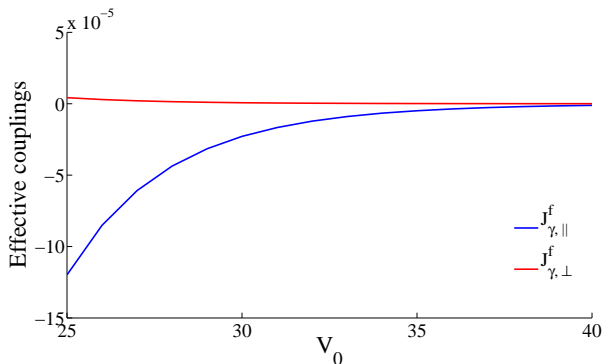


FIG. 11. (Color online) Coefficients of the interaction stemming from the ladder operators in the fermionic case. Notice, in particular, the  $XXZ$ -like type of couplings, which differ from the  $XYZ$ -like couplings obtained for the same terms in the bosonic case (see Fig. 6).

on application of flavor wave theory to the case with antiferromagnetic couplings [15]. These studies confirm the prediction of a highly degenerate manifold of ground-states with both 2- and 3- sublattice ordering for the square and cubic lattices, whose degeneracy is lifted by a mechanism of order-by-disorder [1, 2].

This is an example of the many interesting phenomena that can be experimentally explored with the systems discussed here. In fact, since the Hamiltonian Eq. (33) corresponds to that of an  $XXZ$ -like  $SU(3)$  Heisenberg model, the  $XXZ$ -type of anisotropy will most likely lead to a rich phase diagram for the corresponding ground state, as is the case in  $SU(2)$  Heisenberg models (see [21], for example). The flavor-wave analysis of this system in the  $3D$  lattice is however left for the future.

By increasing the depth of the lattice sites in one of the directions, say  $z$ , so as to suppress the tunneling but still keeping the degeneracy between the different orbital states, it is possible to study the physics of  $2D$  lattices [22]. As reported in [1, 2], the physics here should include the formation of 2- and 3-sublattice ordering, with preference for the 2-sublattice ordering at energies below the energy scale of exchange processes. By increasing the depth of the tunneling in two directions while still keeping the degeneracy between the three orbital states, different types of chains can then be obtained. For example, if the tunneling is restricted to the  $z$ -direction, the effective Hamiltonian will not contain contributions from  $h_3^f$ , and the contributions stemming from the term with the  $J_{38,\sigma}^f$  coupling will cancel due to symmetry. By allowing the dynamics in only  $x$  or only  $y$  directions, the effective Hamiltonian will pick contributions of all terms and it is therefore possible to study antiferromagnetic  $XXZ$ -like  $SU(3)$  models in external fields.

Ferromagnetic  $SU(3)$  Heisenberg models can also be engineered in  $1D$  and  $2D$  by considering the bosonic system, and suppressing the dynamics in 2 or 1 directions, respectively. The main difference, however, is the  $XYZ$

type of anisotropy in the couplings derived from the ladder operators. The same as in the fermionic case, and in analogy to the situation in  $SU(2)$  Heisenberg models, this coupling anisotropy is expected to give rise to very rich physics. To leading order, an effective  $2D$  system obtained from suppressing the dynamics in the  $x$  or  $y$  direction, for example, will contain contributions of both the term of the free field  $h_3^b$  and of the interaction term with coupling  $J_{38}^b$ . This scenario is closer to that recently reported in Ref. [11], which predicts the existence of spiral spin textures in the ground-states of ferromagnetic  $SU(3)$  Heisenberg models. In the  $p$  band system, this would be cast as a rotation (or change in the relative angle of the onsite orbital orientations) of one of the orbital states at each lattice site. We expect that similar physics will appear in the  $1D$  case.

#### IV. EXPERIMENTAL PROBES

The physics discussed here takes place deep in the Mott insulator phase, where single sites of the optical lattice can be accurately approximated by a harmonic potential with frequency  $\omega_\alpha = \sqrt{2V_\alpha k_\alpha^2/m}$  (recall that  $k_\alpha$  are the wave vectors of the optical lattice laser in the direction  $\alpha$ ) [23]. Different vibrational levels in this potential, which in the context of the optical lattices correspond to the different bands, can then be coupled by performing stimulated Raman transitions in a two-level atom [24]. This technique has been employed in Ref. [24] for promoting atoms from the  $s$  to  $p$  bands, in the Mott phase, of  $1D$ ,  $2D$  and  $3D$  lattices. However, since the main object of that study was concerned with the properties of coherence, i.e., the superfluid phase, further manipulation of orbital degrees of freedom in the Mott phase have not been discussed. We therefore extend the methods introduced in [14] for control and manipulation of  $SU(2)$  Heisenberg models based on orbital degrees of freedom, for the implementation of  $SU(3)$  Heisenberg models.

Consider a Raman coupling between the  $|1\rangle = |F=1\rangle$  and  $|2\rangle = |F=2\rangle$  atomic electronic states of  $^{87}\text{Rb}$ . These are two-photon processes where the two levels are coupled with an intermediate virtual state, far detuned from all the other states of the system [24]. Because of this intermediate coupling, implementation of Raman transitions require the use of two different lasers, whose corresponding wave vectors are denoted here by  $\vec{k}_{L_1}$  and  $\vec{k}_{L_2}$ . The matrix element characterizing this transition is given by

$$\frac{\Omega_1 \Omega_2^*}{\delta} \langle 2 | e^{i(\vec{k}_{L_1} - \vec{k}_{L_2}) \cdot \vec{x}} | 1 \rangle, \quad (34)$$

where  $\Omega_i$  are the Rabi frequencies between the  $|i\rangle$  states,  $i = 1, 2$  with another far detuned auxiliary state of this system, say  $|aux\rangle$ , and  $\delta$  is the detuning between  $|aux\rangle$  and the virtual intermediate state.

After adiabatic elimination of the auxiliary state, the interaction between the atom in the harmonic poten-



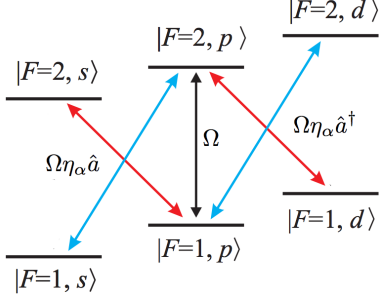


FIG. 12. (Color online) Schematic couplings between the different orbital states. While the carrier transition does not change the vibrational state of the atom, red and blue sideband transitions can be used to lower and raise the vibrational states of the atom, which therefore couples different orbital states.

tial with the lasers driving the Raman coupling is given by [23]

$$H = \sum_{\alpha} \omega_{\alpha} \hat{a}^{\dagger} a - \sum_{\alpha} \left[ \frac{\Delta_{\alpha}}{2} \sigma_z + \frac{1}{2} \Omega \left( \sigma_{+} e^{i\eta_{\alpha}(\hat{a} + \hat{a}^{\dagger})} + h.c. \right) \right], \quad (35)$$

where first term accounts for the center of mass motion of the atom in the harmonic potential, and the second and third terms describe the driven two-level system in the rotating-wave approximation [23]. In this notation  $\Omega = \Omega_1 \Omega_2^* / \delta$  is the effective Rabi frequency,  $\sigma_{+} = (\sigma_{-})^{\dagger} = |2\rangle\langle 1|$ ,  $\sigma_z = |2\rangle\langle 2| - |1\rangle\langle 1|$ ,  $\Delta_{\alpha} = \omega_{\alpha} - \omega_{12}$  are the detunings of the lasers with respect to the atomic transition, of frequency  $\omega_{12}$ , and  $\eta_{\alpha} = \Delta k_{L,\alpha} \sqrt{\hbar/2m\omega_{\alpha}}$  is the Lamb-Dicke parameter, with  $\Delta k_{L,\alpha} = k_{L1,\alpha} - k_{L2,\alpha}$ .

In the Lamb-Dicke regime, when  $\eta_{\alpha} \ll 1$ , the expansion of the exponential can be truncated to  $e^{i\eta_{\alpha}(\hat{a} + \hat{a}^{\dagger})} \approx 1 + i\eta_{\alpha}(\hat{a} + \hat{a}^{\dagger})$  [23], and the corresponding Hamiltonian describes a two-level system coupled to the phonon excitations of the harmonic oscillator with bare Hamiltonian given by  $H_0 = \hat{a}^{\dagger} a - \frac{1}{2} \Delta_{\alpha} \sigma_z$ . The eigenstates of this system can be denoted by  $|1, n\rangle$  and  $|2, n\rangle$ , where  $n$  labels the vibrational level. By carefully choosing the driver frequency, three possible transitions can be implemented [23]: The carrier transition, when  $\Delta_{\alpha} = 0$ ,

$$H_{car} = \frac{\hbar}{2} \Omega [\sigma_{+} + h.c.], \quad (36)$$

which has no effect in the vibrational state. By choosing  $\Delta_{\alpha} = -\omega_{\alpha}$ , the red sideband transitions

$$H_{rsb} = \frac{\hbar}{2} \Omega \eta_{\alpha} [\hat{a}(\sigma_{-})^{\dagger} + \hat{a}^{\dagger} \sigma_{-}] \quad (37)$$

decrease the vibrational state  $n$  by one quanta, when the atom swaps from  $|1\rangle$  to  $|2\rangle$ . Finally, when  $\Delta_{\alpha} = \omega_{\alpha}$  one implement blue sideband transitions,

$$H_{bsb} = \frac{\hbar}{2} \Omega \eta_{\alpha} [\hat{a}^{\dagger}(\sigma_{-})^{\dagger} + \hat{a} \sigma_{-}], \quad (38)$$

that increase the vibrational level  $n$  by one for the same atomic transition. These transitions are schematically shown in Fig. 12. In addition to selective transitions, it is also possible to selectively address the different orbital states [25].  $p_x$  orbitals, for example, can be addressed by choosing driver lasers with no component in the  $y$  and  $z$  directions, i.e.,  $\vec{k}_{L1} - \vec{k}_{L2} = k_{Lx}$ . Analogous relations hold for manipulations of only  $p_y$  and/or  $p_z$  orbitals.

Finally, we show that these (trapped ion based) techniques allow for complete control of these systems by discussing the schemes for implementation of arbitrary rotations. They are performed here by the generators of the  $SU(3)$  group, and for a given effective angle  $\phi$ ,  $\hat{R}_{\beta}(\phi) = e^{-i\lambda_{\beta}\phi/2}$ , with  $\beta = 1, \dots, 8$ . The simplest case, of rotations with  $\lambda_8$ , can be achieved via Stark shift of the  $p_z$  orbital without any disturbance of  $p_x$  and  $p_y$  orbitals.  $\hat{R}_3(\phi)$  rotations are also implemented via Stark shift, but now with a dispersive coupling between both  $p_x$  and  $p_y$  orbitals which already renders the shift with correct (opposite) sign.  $\hat{R}_1(\phi)$ ,  $\hat{R}_4(\phi)$  and  $\hat{R}_6(\phi)$  rotations are implemented by driving red sideband transitions off-resonantly, for two orbitals. The first case will involve the  $p_x$  and  $p_y$  orbitals, while in the second and third,  $p_x$  and  $p_z$ , and  $p_y$  and  $p_z$  orbitals, respectively. The other three rotations, around  $\lambda_2$ ,  $\lambda_5$  and  $\lambda_7$  can be achieved by noticing that  $\hat{R}_2(\phi) = \hat{R}_3(\pi/2)\hat{R}_1(\phi)\hat{R}_3(-\pi/2)$ ,  $\hat{R}_5(\phi) = \hat{R}_3(\pi)\hat{R}_8(-\sqrt{3}\pi)R_4(\phi)\hat{R}_3(-\pi)\hat{R}_8(\sqrt{3}\pi)$ , and  $\hat{R}_7(\phi) = \hat{R}_3(\pi/2)\hat{R}_8(\sqrt{3}\pi/2)R_6(\phi)\hat{R}_3(-\pi/2)\hat{R}_8(-\sqrt{3}\pi/2)$ . Furthermore, the states of pseudospins can be resolved with single-site fluorescence after measurement of  $\lambda_3$  for  $p_x$  and  $p_y$ , and of  $\lambda_8$  for the  $p_z$  orbital. Likewise,  $\langle \lambda_{\alpha} \lambda_{\beta} \rangle$  correlation functions can be obtained by using the same techniques, but now combined with coincident measurement of the fluorescent photons.

Two final remarks regarding experimental feasibility are now in order. First, that as reported in Ref. [24], after the process of loading, the atoms in the  $p$  band remain in a metastable state. The leading decaying channel here stem from atom-atom collisions [12], and therefore the conditions of the Mott<sub>1</sub> phase should corroborate to extending the lifetimes of these systems. Typical lifetimes are estimated to be  $\sim 5$  ms [14]. This is of the order or dozens tunneling times and should therefore allow for experimental probing of the properties discussed here. Second, that although the temperatures required for observation pseudospin correlations derived from exchange interaction are of the order of  $k_B T \lesssim t^{\alpha} t^{\beta} / U_{\alpha\alpha} \sim 10^{-9}$  K, the increased tunneling rates of the  $p$  band may offer slight advantage as compared to the realizations proposed with atoms in the ground band. Nevertheless, these temperatures are still in the frontier achieved by current experiments.

## V. IMPERFECTIONS DUE TO THE LOADING TO THE $p$ BAND

Another challenge with implementation of the effective models is related to experimental imperfections in the process of loading atoms to the  $p$  band. The techniques used in Ref. [24], based on stimulated Raman transitions reported 80% fidelity in promoting the atoms from the  $s$  band in the Mott phase. Therefore it is important to understand how the presence of residual  $s$ -orbital atoms affect the physics of the system.

Let us start by considering

$$U_{sp\alpha} = U_0 \int d\vec{r} |\psi_{sj}(\vec{r})|^2 |\psi_{\alpha j}(\vec{r})|^2, \quad (39)$$

which characterize the strength of repulsive interactions between an  $s$ - and a  $p_\alpha$ -orbital atom at the site  $j$ . Since the  $p_\alpha$ -orbital wave functions are spatially broader than the  $s$ -orbital wave functions,  $U_{sp\alpha} > U_{\alpha\beta}$ , which makes the repulsive interaction between  $s$ -orbital and  $p$ -orbital atoms larger than the repulsive interaction when both atoms are in the  $p$  band. Now two additional processes should be considered in the effective model. The first one, which includes tunneling of  $s$ -orbital atoms, can be safely neglected due to the reduced rate of tunneling in the  $s$  band and the larger value of the coupling constant for repulsive interaction  $U_{sp}$ . The second process, which involves tunneling of  $p_\alpha$ -orbital atoms, will contribute to the Hamiltonian with the following term

$$-\frac{|t_{ij}^\alpha|^2}{U_{sp}} \hat{a}_{\alpha,i}^\dagger \hat{a}_{s,j}^\dagger \hat{a}_{\alpha,i} \hat{a}_{\alpha,j} = -\frac{|t_{ij}^\alpha|^2}{U_{sp}} \hat{n}_{\alpha,i}, \quad (40)$$

where  $\hat{a}_{s,j}$  ( $\hat{a}_{s,j}^\dagger$ ) annihilate (create) an  $s$ -orbital atom at the site  $j$  and where we used that  $\hat{n}_{s,j} = 1$ . The presence of residual  $s$ -orbital atoms is therefore associated with local fluctuations of the external fields, which in this model are represented by the  $\lambda_{3,j}$  and  $\lambda_{8,j}$  Gell-Mann matrices. This means that the effective Hamiltonian contains the additional term

$$H_{dis} = \frac{\sqrt{3}}{6U_{sp}} \lambda_{8,i} \left[ |t_{ij}^x|^2 + |t_{ij}^y|^2 - 2|t_{ij}^z|^2 \right] + \frac{\lambda_{3,i}}{2U_{sp}} \left[ |t_{ij}^x|^2 - |t_{ij}^y|^2 \right]. \quad (41)$$

Notice, here, that in the same way that the coefficients of the external fields derived in Eqs. (31) and (33) were direction dependent, the tunneling anisotropy implies a direction-dependent local shift of the external fields due to  $s$ -atom impurities. Isotropic cubic lattices, however, have vanishing contributions of the  $\lambda_{3,i}$  terms.

Since the loading of atoms to the  $p$  band is implemented globally, a coherent loading will prepare translationally invariant states with a fraction of the population in the  $s$  band. However, whenever the loading is not perfectly coherent, we may envision situations where decoherence process lock the  $s$ -band atoms at fixed sites. In such cases, the collapse of the state describing these

residual atoms, induced by decoherence, will break the translational symmetry and the overall effect of the  $s$ -band atoms will be that of a static disorder in the fields as in Eq. (41). In light of the Imry-Ma argument [26], which establishes a criteria for the stability of ordered phases in the presence of disorder, we expect the presence of  $s$ -atom impurities to have a larger effect in the fermionic system and for effective dynamics in 1D and 2D. The presence of discrete symmetries in the bosonic case should attenuate the effects of impurities even in lower dimensions, and in this case we expect the physics discussed here to be robust even in the presence of  $s$ -orbital atoms.

## VI. CONCLUSIONS

In this paper we presented an alternative controllable system for implementation of different Hamiltonians describing nearest-neighbour interactions between degrees of freedom that are the generators of the  $SU(3)$  group. As explained in the text, the properties of the couplings of the effective models are determined by the statistics of the atoms. Namely, while the effective models associated to the many-body fermionic system contains  $XXZ$ -type of couplings, the effective model associated with the bosonic systems features  $XYZ$ -like anisotropies. By suppressing the dynamics in one or two directions while keeping the degeneracy of the orbital states, it is possible, in addition, to engineer different types of 2D and 1D models.

The systems discussed here allow for quantum simulation of various types of  $SU(3)$  Heisenberg models. Properties of the ground state of the antiferromagnetic case with isotropic couplings have been discussed in the literature, and give rise to very rich physics. This include, for example, the mechanism of order-by-disorder for lifting the degeneracy of a highly degenerate manifold of ground states [1, 2, 15]. In analogy to the situation in  $SU(2)$  Heisenberg models, we expect both the antiferromagnetic  $XXZ$ -like case and the ferromagnetic case with  $XYZ$ -type of couplings to display a rich phase diagram for the ground state. However, characterization of these properties via flavor-wave analysis in the 2D and 3D cases is left for the future.

As a final remark we notice that the perturbative method discussed in Sec. III combined with the experimental probing of Sec. IV can be used as a general tool for deriving quantum simulators of exotic models of magnetism. In this framework, where the pseudospin degree of freedom is encoded in the orbital states of excited bands of optical lattices, properties of the couplings mediating interactions in the corresponding effective model will intrinsically depend on the dynamical processes featured in the many-body system. In this sense, different lattice geometries as e.g. the triangular lattice could lead to interesting effects, specially via the presence of Dzyaloshinskii-Moriya exchange. Furthermore, experi-

mentally controllable  $SU(3)$  systems might be of interest for realization of topological states of matter [27].

## VII. ACKNOWLEDGMENTS

I thank Jonas Larson, Jani-Petri Martikainen, Stephen Powell, Tobias Grass, Thomas Quella and Daniele

Marmioli for helpful discussions. Jonas Larson and Jani-Petri Martikainen are once more acknowledged for comments on the manuscript. The research has been supported by the Swedish research council (VR). This paper is dedicated to A. F. R. de Toledo Piza, on the occasion of his 76<sup>th</sup> birthday.

## Appendix A: $SU(3)$ symmetry

The  $SU(3)$  group has 8 generators, denoted here by  $\lambda_i$ ,  $i = 1..8$ . Explicit expressions (taken from Ref. [20]) are given below, together with the notation used in the text:

$$\begin{aligned} \lambda_z^1 = \lambda_1 &= \begin{pmatrix} 0 & 1 & 0 \\ 1 & 0 & 0 \\ 0 & 0 & 0 \end{pmatrix}, \quad \lambda_z^2 = \lambda_2 = \begin{pmatrix} 0 & -i & 0 \\ i & 0 & 0 \\ 0 & 0 & 0 \end{pmatrix}, \quad \lambda_y^1 = \lambda_4 = \begin{pmatrix} 0 & 0 & 1 \\ 0 & 0 & 0 \\ 1 & 0 & 0 \end{pmatrix}, \quad \lambda_y^2 = \lambda_5 = \begin{pmatrix} 0 & 0 & -i \\ 0 & 0 & 0 \\ i & 0 & 0 \end{pmatrix}, \\ \lambda_x^1 = \lambda_6 &= \begin{pmatrix} 0 & 0 & 0 \\ 0 & 0 & 1 \\ 0 & 1 & 0 \end{pmatrix}, \quad \lambda_x^2 = \lambda_7 = \begin{pmatrix} 0 & 0 & 0 \\ 0 & 0 & -i \\ 0 & i & 0 \end{pmatrix}, \quad \lambda_3 = \begin{pmatrix} 1 & 0 & 0 \\ 0 & -1 & 0 \\ 0 & 0 & 0 \end{pmatrix}, \quad \lambda_8 = \frac{1}{\sqrt{3}} \begin{pmatrix} 1 & 0 & 0 \\ 0 & 1 & 0 \\ 0 & 0 & -2 \end{pmatrix}. \end{aligned} \quad (A1)$$

The Lie algebra of  $SU(3)$  is given by  $[\lambda_i, \lambda_j] = 2if_{ijk}\lambda_k$ , where  $i, j = 1, \dots, 8$   $f_{ijk} = -f_{jik} = -f_{ikj}$  are totally antisymmetric structure constants. The values for the different combinations of indices follow  $f_{123} = 1$ ,  $f_{147} = -f_{156} = f_{246} = f_{257} = f_{345} = -f_{367} = \frac{1}{2}$  and  $f_{458} = f_{678} = \frac{\sqrt{3}}{2}$ .

The  $SU(3)$  group has two Casimir operators,

$$\begin{aligned} C_1(\lambda_i) &= \frac{1}{4} \sum_i \lambda_i^2 \quad \text{and} \\ C_2(\lambda_i) &= \frac{1}{8} \sum_{ijk} d_{ijk} \lambda_i \lambda_j \lambda_k, \end{aligned}$$

where  $d_{118} = d_{228} = d_{338} = -d_{888} = \frac{1}{\sqrt{3}}$ ,  $d_{146} = d_{157} = d_{344} = d_{355} = -d_{366} = -d_{377} = \frac{1}{2}$ , and  $d_{448} = d_{558} = d_{668} = d_{778} = -\frac{1}{2\sqrt{3}}$ .

## Appendix B: Coupling constants

The expressions of the various coupling constants used in the text are given below for both the bosonic and fermionic many-body systems.

### 1. Bosonic case

In the notation below we use  $\sigma$  to denote  $\langle i, j \rangle_\sigma$ . This defines the values of the tunneling amplitudes, which are different for various orbital states in the different directions.

$$J_{8,\sigma}^b = \frac{K_{xx}^{(1)}}{3} |t_{ij}^x|^2 + \frac{K_{yy}^{(1)}}{3} |t_{ij}^y|^2 + \frac{4}{3} K_{zz}^{(1)} |t_{ij}^z|^2 + \frac{K_{xy}^{(2)}}{6} (|t_{ij}^x|^2 + |t_{ij}^y|^2) - \frac{2}{9} K_{xz}^{(2)} (|t_{ij}^x|^2 + |t_{ij}^z|^2) - \frac{2}{9} K_{yz}^{(2)} (|t_{ij}^y|^2 + |t_{ij}^z|^2) \quad (B1)$$

$$J_{3,\sigma}^b = K_{xx}^{(1)} |t_{ij}^x|^2 + K_{yy}^{(1)} |t_{ij}^y|^2 - \frac{K_{xy}^{(2)}}{2} (|t_{ij}^x|^2 + |t_{ij}^y|^2) \quad (B2)$$

$$J_{38,\sigma}^b = \frac{\sqrt{3}}{3} K_{xx}^{(1)} |t_{ij}^x|^2 - \frac{\sqrt{3}}{3} K_{yy}^{(1)} |t_{ij}^y|^2 - \sqrt{3} \frac{K_{xz}^{(2)}}{6} (|t_{ij}^x|^2 + |t_{ij}^z|^2) + \sqrt{3} \frac{K_{yz}^{(2)}}{6} (|t_{ij}^y|^2 + |t_{ij}^z|^2) \quad (B3)$$

$$J_{\gamma,\sigma}^1 = K_{\alpha\beta}^{(1)} t_{ij}^\alpha t_{ij}^\beta + 2K_{\alpha\beta}^{(2)} t_{ij}^\alpha t_{ij}^\beta \quad (\text{B4})$$

$$J_{\gamma,\sigma}^2 = K_{\alpha\beta}^{(1)} t_{ij}^\alpha t_{ij}^\beta - 2K_{\alpha\beta}^{(2)} t_{ij}^\alpha t_{ij}^\beta \quad (\text{B5})$$

$$h_{8,\sigma}^b = 4\frac{\sqrt{3}}{9}K_{xx}^{(1)}|t_{ij}^x|^2 + 4\frac{\sqrt{3}}{9}K_{yy}^{(1)}|t_{ij}^y|^2 - 8\frac{\sqrt{3}}{9}K_{zz}^{(1)}|t_{ij}^z|^2 - \frac{\sqrt{3}}{9}K_{xy}^{(2)}(|t_{ij}^x|^2 + |t_{ij}^y|^2) - \frac{\sqrt{3}}{9}K_{yz}^{(2)}(|t_{ij}^y|^2 + |t_{ij}^z|^2) \quad (\text{B6})$$

$$h_{3,\sigma}^b = \frac{4}{3}K_{xx}^{(1)}|t_{ij}^x|^2 - \frac{4}{3}K_{yy}^{(1)}|t_{ij}^y|^2 + \frac{K_{xz}^{(2)}}{3}(|t_{ij}^x|^2 + |t_{ij}^z|^2) - \frac{K_{yz}^{(2)}}{3}(|t_{ij}^y|^2 + |t_{ij}^z|^2) \quad (\text{B7})$$

## 2. Fermionic case

In the same way as for the bosonic case discussed above,  $\sigma$  is used below to define the value of the tunneling amplitudes.

$$J_{8,\sigma}^f = \frac{K_{xy}^{(2)}}{6}(|t_{ij}^x|^2 + |t_{ij}^y|^2) - 2\frac{K_{xz}^{(2)}}{9}(|t_{ij}^x|^2 + |t_{ij}^z|^2) - 2\frac{K_{yz}^{(2)}}{9}(|t_{ij}^y|^2 + |t_{ij}^z|^2) \quad (\text{B8})$$

$$J_{3,\sigma}^f = -\frac{K_{xy}^{(2)}}{2}(|t_{ij}^x|^2 + |t_{ij}^y|^2) \quad (\text{B9})$$

$$J_{38,\sigma}^f = -\sqrt{3}\frac{K_{xz}^{(2)}}{6}(|t_{ij}^x|^2 + |t_{ij}^z|^2) + \sqrt{3}\frac{K_{yz}^{(2)}}{6}(|t_{ij}^y|^2 + |t_{ij}^z|^2) \quad (\text{B10})$$

$$J_{\gamma,\sigma}^f = t_{ij}^\alpha t_{ji}^\beta K_{\alpha\beta}^{(2)} \quad (\text{B11})$$

$$h_{8,\sigma}^f = 2\frac{\sqrt{3}}{9}K_{xy}^{(2)}(|t_{ij}^x|^2 + |t_{ij}^y|^2) - \frac{\sqrt{3}}{9}K_{xz}^{(2)}(|t_{ij}^x|^2 + |t_{ij}^z|^2) - \frac{\sqrt{3}}{9}K_{yz}^{(2)}(|t_{ij}^y|^2 + |t_{ij}^z|^2) \quad (\text{B12})$$

$$h_{3,\sigma}^f = \frac{K_{xz}^{(2)}}{3}(|t_{ij}^x|^2 + |t_{ij}^z|^2) - \frac{K_{yz}^{(2)}}{3}(|t_{ij}^y|^2 + |t_{ij}^z|^2) \quad (\text{B13})$$

- 
- [1] T. A. Tóth, A. M. Läuchli, F. Mila, and K. Penc, “Three-sublattice Ordering of the SU(3) Heisenberg Model of Three-Flavor Fermions on the Square and Cubic Lattices,” *Physical Review Letters*, vol. 105, no. 26, p. 265301, 2010.
- [2] B. Bauer, “Three-sublattice Order in the SU(3) Heisenberg Model on the Square and Triangular Lattice,” *Physical Review B*, vol. 85, no. 12, 2012.
- [3] Y. Li, “ $su(4)$  theory for spin systems with orbital degeneracy,” *Physical Review Letters*, vol. 81, no. 16, pp. 3527–3530, 1998.
- [4] J. Simon, W. S. Bakr, R. Ma, M. E. Tai, P. M. Preiss, and M. Greiner, “Quantum Simulation of Antiferromagnetic Spin Chains in an Optical Lattice,” *Nature*, vol. 472, no. 7343, pp. 307–312, 2011.
- [5] J. Struck, M. Weinberg, C. Ölschläger, P. Windpassinger, J. Simonet, K. Sengstock, R. Höppner, P. Hauke,

- A. Eckardt, M. Lewenstein, *et al.*, “Engineering Ising-XY Spin-models in a Triangular Lattice Using Tunable Artificial Gauge Fields,” *Nature Physics*, vol. 9, no. 11, pp. 738–743, 2013.
- [6] J. S. Krauser, U. Ebling, N. Fläschner, J. Heinze, K. Sengstock, M. Lewenstein, A. Eckardt, and C. Becker, “Giant Spin Oscillations in an Ultracold Fermi Sea,” *Science*, vol. 343, no. 6167, pp. 157–160, 2014.
- [7] U. Ebling, J. S. Krauser, N. Fläschner, K. Sengstock, C. Becker, M. Lewenstein, and A. Eckardt, “Relaxation Dynamics of an Isolated Large-Spin Fermi Gas Far from Equilibrium,” *Physical Review X*, vol. 4, no. 2, p. 021011, 2014.
- [8] C. Honerkamp and W. Hofstetter, “Ultracold Fermions and the SU(N) Hubbard model,” *Physical Review Letters*, vol. 92, no. 17, p. 170403, 2004.
- [9] C. Senko, P. Richerme, J. Smith, A. Lee, I. Cohen, A. Retzker, and C. Monroe, “Experimental Realization of a Quantum Integer-Spin Chain with Controllable Interactions,” *arXiv preprint arXiv:1410.0937*, 2014.
- [10] T. Graß, B. Juliá-Díaz, M. Kuś, and M. Lewenstein, “Quantum Chaos in SU(3) Models With Trapped Ions,” *Physical Review Letters*, vol. 111, no. 9, p. 090404, 2013.
- [11] T. Graß, R. W. Chhajlany, C. A. Muschik, and M. Lewenstein, “Spiral Spin Textures of Bosonic Mott Insulator with SU(3) Spin-Orbit Coupling,” *arXiv preprint arXiv:1408.0769*, 2014.
- [12] A. Isacsson and S. Girvin, “Multiflavor Bosonic Hubbard Models in the First Excited Bloch Band of an Optical Lattice,” *Physical Review A*, vol. 72, no. 5, p. 053604, 2005.
- [13] M. Lewenstein and W. V. Liu, “Optical lattices: Orbital Dance,” *Nature Physics*, vol. 7, pp. 101–103, 2011.
- [14] F. Pinheiro, G. M. Bruun, J.-P. Martikainen, and J. Larson, “XYZ Quantum Heisenberg Models with  $p$ -Orbital Bosons,” *Physical Review Letters*, vol. 111, no. 205302, 2013.
- [15] N. Papanicolaou, “Unusual Phases in Quantum Spin-1 Systems,” *Nuclear Physics B*, vol. 305, no. 3, pp. 367–395, 1988.
- [16] F. Pinheiro, J.-P. Martikainen, and J. Larson, “Confined  $p$ -band Bose-Einstein Condensates,” *Physical Review A*, vol. 85, no. 3, p. 033638, 2012.
- [17] N. Mermin, “Absence of Ferromagnetism or Antiferromagnetism in One- or Two-Dimensional Isotropic Heisenberg Models,” *Physical Review Letters*, vol. 17, no. 22, pp. 1133–1136, 1966.
- [18] P. Hohenberg, “Existence of Long-Range Order in One and Two Dimensions,” *Physical Review*, vol. 158, no. 2, pp. 383–386, 1967.
- [19] A. Auerbach, *Interacting Electrons and Quantum Magnetism*. Springer Verlag, 1994.
- [20] W. Greiner and B. Müller, *Quantum Mechanics: Symmetries*, vol. 2. Springer, 1994.
- [21] H.-J. Mikeska and A. K. Kolezhuk, “One-dimensional Magnetism,” in *Quantum Magnetism*, pp. 1–83, Springer, 2004.
- [22] X. Li, Z. Zhang, and W. V. Liu, “Time-Reversal Symmetry Breaking of  $p$ -Orbital Bosons in a One-Dimensional Optical Lattice,” *Physical Review Letters*, vol. 108, no. 17, p. 175302, 2012.
- [23] S. Haroche and J.-M. Raimond, *Exploring the Quantum: Atoms, Cavities, and Photons (Oxford Graduate Texts)*. Oxford University Press, USA, 2013.
- [24] T. Müller, S. Fölling, A. Widera, and I. Bloch, “State Preparation and Dynamics of Ultracold Atoms in Higher Lattice Orbitals,” *Physical Review Letters*, vol. 99, no. 20, p. 200405, 2007.
- [25] W. S. Bakr, J. I. Gillen, A. Peng, S. Fölling, and M. Greiner, “A Quantum Gas Microscope for Detecting Single Atoms in a Hubbard-regime Optical Lattice,” *Nature*, vol. 462, no. 7269, pp. 74–77, 2009.
- [26] Y. Imry and S.-k. Ma, “Random-field Instability of the Ordered State of Continuous Symmetry,” *Physical Review Letters*, vol. 35, no. 21, p. 1399, 1975.
- [27] R. Barnett, G. Boyd, and V. Galitski, “SU(3) Spin-Orbit Coupling in Systems of Ultracold Atoms,” *Physical Review Letters*, vol. 109, no. 23, p. 235308, 2012.